J. Fluid Mech. (1974), *vol.* 62, *part* 1, *pp.* 85–114
Printed in Great Britain

Response of Pitot probes in turbulent streams

By H. A. BECKER AND A. P. G. BROWN
Department of Chemical Engineering, Queen's University, Kingston, Ontario

(Received 24 May 1972 and in revised form 4 June 1973)

The response of a Pitot probe in a uniform laminar stream is commonly expressed in the form

$$P_s = P + \tfrac{1}{2}C\rho U^2,$$

where P_s is the probe signal pressure, P is the stream static pressure, U is the stream speed and ρ is the fluid density. It has been found that for ordinary sphere-nosed, round-nosed and square-nosed probes

$$1 - C = K(\sin^2\theta)^m = K(U_n^2/U^2)^m,$$

where θ is the angle between the velocity vector and the probe axis, and $U_n \equiv U\sin\theta$ is the transverse velocity component. The parameters m and K are functions of the probe geometry. These formulae also describe the performance in a turbulent stream when the probe is small compared with the turbulence scale. The evaluation of the time-averaged response is treated, and an answer is developed to the question of what it is that a Pitot probe measures in a turbulent stream. In a turbulent shear flow having the properties of a boundary layer, the reference pressure is best taken to be the static pressure at the shear-layer edge. It is shown that round-nosed probes with $D_i/D \simeq 0{\cdot}45$ and square-nosed probes with $D_i/D \simeq 0{\cdot}15$ then detect $\frac{1}{2}\rho\overline{U}_x^2$ with good accuracy, where D_i/D is the ratio of the inside and outside diameters of the Pitot tube. When measurements are made with two probes of dissimilar geometry, the differential response can be used to find the mean-square level of the transverse velocity fluctuations. Turbulence levels so measured agree closely with results from hot-wire anemometry.

1. Introduction

The effect of turbulence on the response of Pitot probes has excited speculation (e.g. Goldstein 1936; Hinze & van der Hegge Zijnen 1949; Alexander, Baron & Comings 1950) but little serious study, despite the widespread use of the device to measure mean velocity turbulent flows. We have used Pitot probes in studies of turbulent jets and flames, and have been conscious of the considerable uncertainty in the interpretation of the results in regions of high turbulence intensity. It also occurred to us (1969) that any effect of turbulence might be used for the characterization of turbulent velocity fluctuations. The present investigation was therefore undertaken, first, to advance the knowledge of Pitot response in turbulent flows and second, to examine the use of Pitot devices for the detection of turbulence intensity.

The basis for a quantitative treatment of the problem was established by Hinze (1959, p. 136), whose argument suggests that the theory of the response in a turbulent stream, where the velocity vector fluctuates in both magnitude and direction, should be based on knowledge of the directional response in a laminar stream. He supposed that in a laminar flow

$$P_s - P = \tfrac{1}{2}\rho U^2[1 - B(1 - \cos\theta)], \tag{1}$$

where θ is the angle between the velocity vector and the probe axis, and B is a constant. In a turbulent flow

$$\cos\theta = U_x/U = (\bar{U}_x + u_x)/(\bar{U}_x^2 + u_x^2 + u_y^2 + u_z^2)^{\frac{1}{2}}.$$

On applying a series expansion and time averaging the result, he obtained

$$\bar{P}_s - \bar{P} = \tfrac{1}{2}\bar{U}_x\left[1 + \frac{\overline{u_x^2} + \overline{u_y^2} + \overline{u_z^2}}{\bar{U}_x^2} - B\left(\frac{\overline{u_y^2} + \overline{u_z^2}}{2\bar{U}_x^2} + \frac{\overline{u_y^4} + \overline{u_z^4} + 2\overline{u_y^2 u_z^2}}{8\bar{U}_x^2} + \ldots\right)\right]. \tag{2}$$

Hackeschmidt (1968) and Eickhoff (1969) have examined the application of this relation, and the latter has reported experimental values of B for several probes.

The present work shows that (1) and (2) can be considerably improved with respect to generality and accuracy, and better results are obtained by using a different laminar response equation and a more rigorous statistical scheme. The basic idea underlying the analysis is, however, the same. It consists of the assumption, implicit in Hinze's approach, that, when the turbulence scale is large compared with the critical probe dimensions, the flow around the probe is locally quasi-steady, quasi-uniform and quasi-laminar and the instantaneous signal pressure in the probe head is virtually the same as in a steady uniform laminar stream. The time-mean response is then formed by time averaging the instantaneous signal. This is analogous to the approach in hot-wire anemometry, where it is supposed that the law of heat loss at any instant from a sufficiently small heated cylinder in a turbulent stream is the same as in a steady laminar flow with the same local velocity. The assumption must be valid in the limit. Otherwise, it must largely be left to experiment to establish quantitatively the conditions under which it fails; i.e. when is the turbulence scale too small relative to the probe dimensions, and how do the frequency response characteristics of the probe affect the result?

The work followed the plan suggested by the above discussion. A study was made of the directional response of Pitot probes in a steady uniform laminar stream, and a general formula for the response characteristic was developed. An expression for the time-mean response in a statistically steady turbulent stream was then obtained by time averaging, and mathematical solutions were developed under a set of simplifying assumptions. The results were used (i) to explore the optimization of probes for mean velocity measurements in turbulent flows and (ii) to examine the possibilities for the detection of velocity fluctuation intensity. The predictions were finally compared with experimental data and shown to be practically valid.

2. General considerations

Attention is restricted to probes that are axisymmetric. A Cartesian (x, y, z) reference frame is generally convenient, with origin at the centre of the probe mouth, Ox along the probe axis and x positive in the direction into the probe.

Since the plane of the probe mouth is perpendicular to the probe axis, the angle θ between the axis and the stream velocity **U** can be unambiguously called the angle of incidence of **U** on the probe (rather than, arbitrarily, yaw or pitch). The velocity **U** may be resolved into $U_x \equiv U\cos\theta$ and $U_n \equiv \sin\theta$. The component U_n is outward, normal to the probe axis and represents the stream speed in the plane of the probe mouth, analogous to the three-dimensional stream speed U. We have $U_n^2 \equiv U_y^2 + U_z^2$ and $U^2 \equiv U_x^2 + U_y^2 + U_z^2$.

Consider a probe in a steady uniform laminar stream. Not far inside the probe, the influence of the external flow effectively vanishes and the fluid is at rest. The quantity sensed in a measurement is the pressure P_s within this stagnant fluid. The pressure in the undisturbed field at the position of the centre of the probe mouth (when the probe is absent) is P, the stagnation pressure is P_0, and the stream velocity is **U**. When $P_s = P_0$, the response is commonly held to be ideal, a notion reflected in the name 'total head probe'. Then $P_s - P = P_0 - P = \frac{1}{2}\rho U^2$ and the instrument detects the stream speed U.

In view of the most frequent objective of velocity measurements, it might be more desirable for the definition of ideal response to be $P_s - P = \frac{1}{2}\rho U_x^2 = \frac{1}{2}\rho U^2 \times (1 - \sin^2\theta)$. Such a response is, however, unobtainable, whereas $P_s - P = \frac{1}{2}\rho U^2$ is closely approached by certain probe designs over a wide range of θ, and represents the upper limit in a uniform laminar stream. The custom of using

$$P_s - P = \tfrac{1}{2}\rho U^2$$

as a reference standard will therefore be retained, but with the following qualification: we shall call it the ideal *total* response. We shall then introduce the concept of ideal *transverse* response, defined by

$$P_s - P = \tfrac{1}{2}\rho U^2(1 - K\sin^2\theta), \tag{3}$$

where K is a constant. Thus a probe with ideal transverse response is one whose departure from ideal total response is linear in $\sin^2\theta \equiv U_n^2/U^2$.

Dynamic effects of the measurement system and of the pressure transmission lines do not exist under the condition that the fluid inside the probe, beyond the immediate vicinity of the probe mouth, is stagnant, and the output signal is the pressure P_s within this fluid. This restriction is in accord with good measurement practice; calibration for conditions where significant surging of fluid through the probe is allowed is usually difficult or impossible and is not normally attempted. In steady laminar flows, the problem should not arise. For statistically stationary turbulent flows, interest is restricted to the time mean of P_s; virtual stagnation of the probe fluid is then ensured if the volume of fluid in the line of pressure transmission is adequately small, or if a suitable flow resistance is inserted in the line of transmission at a point sufficiently near the probe mouth. If the instantaneous signal is however to be detected, in a turbulent flow or in any

other fast transient flow, then the flow passage should be blocked not far from the mouth, and a suitable transducer, such as a piezoelectric device, located in the passage to sense the instantaneous value of P_s. Ebrahimi (1967) has reported on a probe in which a condenser microphone was used.

3. The effect of orientation in laminar flow

Four external probe geometries will be considered: (i) the sphere-nosed probe, a sphere on a tubular support, (ii) the round-nosed probe, a hemispherically truncated tube, (iii) the square-nosed probe, a squarely truncated tube, and (iv) the sharp-lipped probe, often realized as a conically truncated tube of small cone angle brought to minimum practical thickness at the lip. The characteristic external diameter D is the sphere diameter in the first case, the outside tube diameter in the second two and the outside tip diameter in the last. The probe 'nose' includes the straight run of tube, of length L, before any bends or significant changes in diameter. The scale of the internal geometry is characterized by the mouth diameter D_i of the impact pressure opening. The following conditions are set.

(i) The probe nose is long enough so that downstream geometry has negligible effect on the response. The results of Ower & Johansen (1926) on static pressure distribution along the nose indicate that $L/D > 6$ is normally sufficient.

(ii) The internal passage is of constant diameter for a sufficient distance L_i so that the fluid inside is brought to rest before any changes of cross-section, eliminating internal geometry as a variable. Data on the performance of static pressure taps (Myadzu 1936; Ray 1956) indicate that $L_i/D_i > 3$ is normally sufficient.

(iii) Unless otherwise noted, the probe Reynolds number DU/ν is large and viscous effects are unimportant, admitting arguments from potential-flow theory.

(iv) Unless otherwise noted, the Mach number is small and compressibility effects are unimportant.

The probe response in a uniform laminar flow is usually expressed as

$$P_s - P = \tfrac{1}{2}C\rho U^2. \tag{4}$$

Under the stated conditions, the coefficient C is expected to depend only on the diameter ratio D_i/D and the external geometry. We have found empirically that the following generalization of (3) describes most results within the margins of experimental error:

$$P_s - P = \tfrac{1}{2}\rho U^2(1 - K(\sin^2\theta)^m), \tag{5}$$

where K and m are constants for a given probe. Figure 1 shows typical results for square-nosed and round-nosed probes; in each case the graph of $\ln(1-C)$ *vs.* $\ln(\sin^2\theta)$ puts the data on a straight line, confirming the applicability of (5) over the experimental range of θ. Since (5) provides a very convenient expression of the transverse response, i.e. the response to $\sin^2\theta \equiv U_n^2/U^2$, no other form will be considered. We have $m = 1$ for ideal transverse response, $m = \infty$ for ideal total response and for real probes, $1 < m < \infty$.

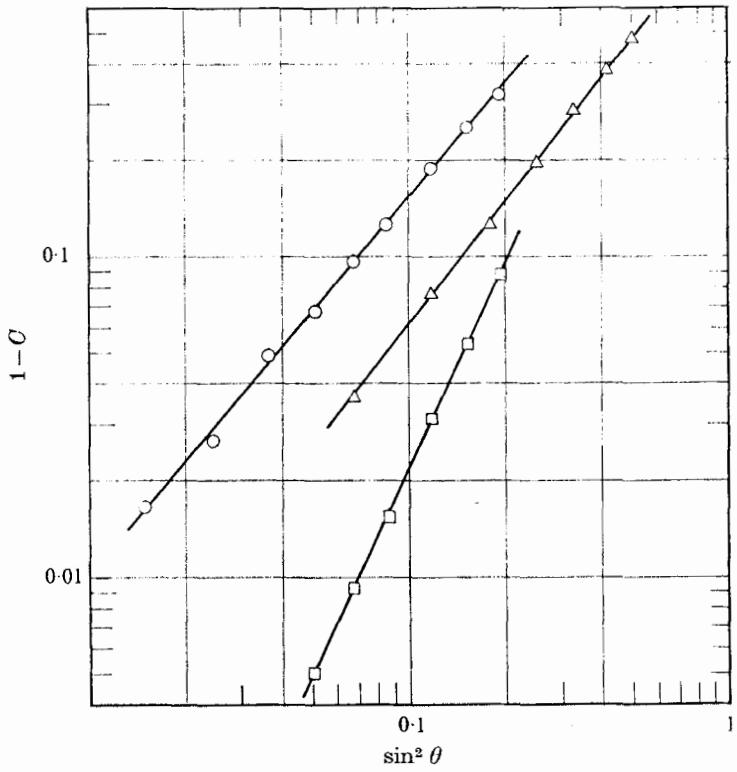

FIGURE 1. Examples of directional response characteristics for Pitot probes, demonstrating applicability of the relation $\ln(1-C) = \ln K + m \ln(\sin^2\theta)$. ○, round-nosed probe with $D_i/D = 0{\cdot}108$ (present work); □, square-nosed probe with $D_i/D = 0{\cdot}125$ (Gracey *et al.* 1951); △, square-nosed probe with $D_i/D = 0{\cdot}61$ (present work).

Results for sphere-nosed, round-nosed and square-nosed probes

A general summary of experimental results is given in table 1 and the values of m and K are also shown graphically in figure 3. Figure 3 was found to be useful in interpolating and extrapolating the results for square-nosed and round-nosed probes. Our sphere-nosed probes were constructed from brass ball-bearings mounted on small hypodermic tubing stems. Further details of our experiments may be found in a thesis (Brown 1971) and in an earlier paper (Becker & Brown 1969).

The values of m and K as functions of the diameter ratio D_i/D (figure 3) can also be estimated from the empirical formulae summarized in table 2. The potential-flow solution for the pressure field around a sphere gives $K = \frac{9}{4}$ and $m = 1$ exactly as $D_i/D \to 0$. For round-nosed and square-nosed probes, the case of the thin-walled tube is approached as $D_i/D \to 1$. Extrapolation indicates that in this limit $m = 3{\cdot}13$ and $K = 2{\cdot}91$.

D_i/D	m	K	K/m	Range of $1-C$		θ_m
			Sphere-nosed (Becker & Brown 1969)			
0·084	1·173	2·05	1·75	0·005	0·5	33°+
			Sphere-nosed (present data)			
0·073	1·140	2·18	1·91	0·005	0·4	28°+
0·095	1·185	2·17	1·83	0·005	0·4	28°+
0·127	1·220	2·15	1·76	0·005	0·3	28°+
0·174	1·307	2·29	1·75	0·005	0·3	28°+
0·226	1·372	2·31	1·68	0·005	0·2	28°+
0·257	1·415	2·27	1·61	0·005	0·2	28°+
			Round-nosed (Merriam & Spaulding 1931)			
0·195	1·495	3·70	2·48	0·01	0·3	24°+
0·295	1·600	3·49	2·18	0·006	0·2	24°+
0·395	1·698	3·41	2·01	0·004	0·2	24°+
0·500	1·764	2·76	1·56	0·003	0·1	24°+
0·740	1·820	1·048	0·58	0·003	0·04	24°+
			Round-nosed (Pankhurst & Holder 1952)			
0·24	1·665	5·08	3·05	0·006	0·15	18°+
0·33	1·683	3·18	1·89	0·008	0·05	20°+
0·53	2·06	4·52	2·19	0·015	0·15	25°+
			Round-nosed (present data)			
0·108	1·192	2·39	2·00	0·01	0·4	28°+
			Square-nosed (Davies 1957)			
0·075	1·265	1·310	1·037	0·015	0·6	45°+
0·409	1·579	1·586	0·995	0·02	0·5	45°+
0·663	1·99	2·20	0·905	0·01	0·5	36°
0·825	2·45	2·65	0·920	0·015	0·5	36°
0·965	3·00	2·79	0·930	0·015	0·4	45°+
			Square-nosed (Gracey *et al.* 1951)			
0·125	1·286	1·142	0·888	0·03	0·5	45°+
			Square-nosed (present data)			
0·61	2·13	2·94	1·38	0·005	0·5	28°+
0·64	2·00	2·04	1·02	0·005	0·5	33°+
			Flat-tipped, tapered (Gracey *et al.* 1951)			
$\alpha = 7{\cdot}5°$, $D_i/D_o = 0{\cdot}125$						
0·385	1·445	1·51	1·04	0·03	0·6	45°+
0·555	1·693	1·99	1·17	0·05	0·6	45°+
1·000	2·77	3·61	1·30	0·02	0·3	SNC
$\alpha = 15°$, $D_i/D_o = 0{\cdot}125$						
0·385	1·301	1·56	1·20	0·04	0·7	45°+
0·555	1·474	1·99	1·35	0·03	0·7	SNC
1·00	2·24	3·61	1·61	0·06	0·7	SNC
$\alpha = 22{\cdot}5°$, $D_i/D_o = 0{\cdot}125$						
0·375	1·221	1·68	1·38	0·05	0·7	SNC
0·555	1·342	2·08	1·55	0·05	0·8	SNC
1·00	1·890	3·54	1·87	0·05	1	SNC

D_i/D	m	K	K/m	Range of $1-C$		θ_m
Flat-tipped, tapered (Merriam & Spaulding 1931)						
N.P.L., $\alpha = 2{\cdot}9°$, $D_i/D_o = 0{\cdot}20$						
0·35	1·686	2·17	1·29	0·01	0·1	24°+
W.N.Y., $\alpha = 5{\cdot}0°$, $D_i/D_o = 0{\cdot}20$						
0·44	2·04	3·62	1·77	0·008	0·1	24°+
B.S., $\alpha = 3{\cdot}4°$, $D_i/D_o = 0{\cdot}38$						
0·84	2·14	1·34	0·63	0·005	0·04	24°+
A.S.H.V.E., $\alpha = 13{\cdot}6°$, $D_i/D_o = 0{\cdot}20$						
0·32	1·787	3·00	1·68	0·01	0·1	24°+

TABLE 1. Response parameters and data ranges in studies of sphere-nosed, round-nosed, square-nosed and tapered Pitot probes. The last column shows the upper limit of the range of θ in which (5) is followed; an entry such as 45°+ means that (5) applied over the entire experimental range, while 'SNC' indicates slight negative curvature over the entire range.

Tapered and sharp-lipped probes

Probes with $D_i/D \simeq 1$ are of particular interest because of their virtually ideal total response over a broad range of θ; for example, figure 2 indicates that $1-C < 0{\cdot}001$ up to 16° and $1-C < 0{\cdot}01$ up to 24°. Square-nosed probes with D_i/D nearly unity are, however, often impractical because of the small wall thickness required. A tube tapered at the tip to the minimum practical lip thickness may then be employed. The question arises as to how steep the taper can be without significantly affecting the response.

Consider therefore a flat-tipped tapered probe – a conically truncated tube, truncated yet again by a plane at right angles. The outer diameter of the tube is D_o, the inner diameter is D_i, the outer tip diameter is D_t, the length of the tapered section is L_t and the taper is characterized by the cone half-angle

$$\alpha = \tan^{-1}((D_o - D_t)/2L_t).$$

In general, the characteristic outside nose diameter may be taken to be either $D = D_o$ or $D = D_t$. When α is sufficiently small, the response should be that of a square-nosed probe with $D = D_t$. At the other extreme, as α approaches a right angle, the probe becomes a square-nosed probe with $D = D_o$. Because of our interest in small values of α, we take $D = D_t$, giving $D_i/D = D_i/D_t$ for the characteristic diameter ratio.

Experimental results for flat-tipped tapered probes are shown in figure 4 and parameter values are summarized in table 1. The results indicate that, when $\alpha < 3°$, the values of m and K differ negligibly from those for square-nosed probes of equal D_i/D. It should be noted that at larger values of α equation (5) was exactly followed in only a few cases. The deviating data sets showed a small but significant negative curvature in the graph of $\ln(1-C)$ *vs.* $\ln(\sin^2\theta)$, and the values of m and K in table 1 were obtained by fitting the best straight line over the range of the data.

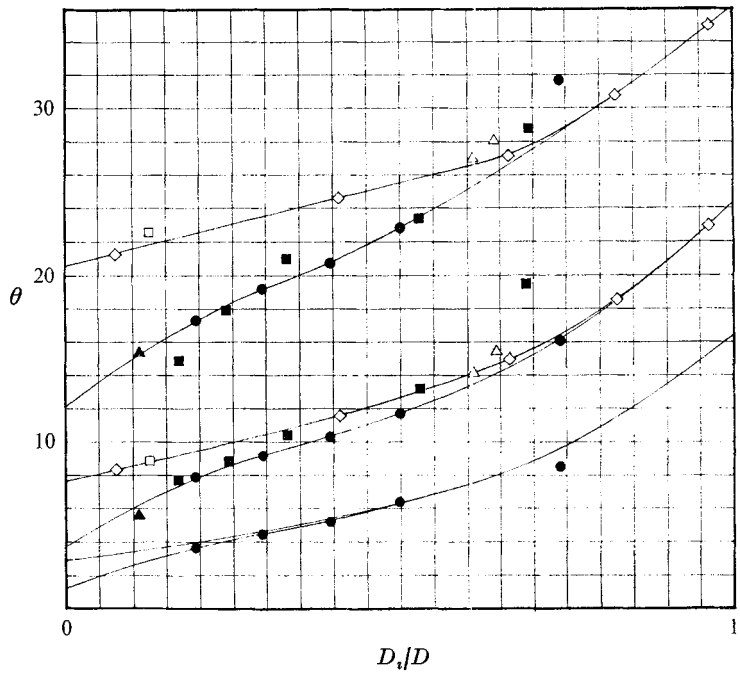

FIGURE 2. A comparison of response characteristics for square-nosed and round-nosed Pitot probes: the angle θ where (top curves) $1-C = 0{\cdot}1$, (middle curves) $1-C = 0{\cdot}01$ and (bottom curves) $1-C = 0{\cdot}001$, as a function of D_i/D. Probe types: ◇, △, square-nosed; ●, ■, ▲, round-nosed. Data sources: ◇, Davies (1957); △, ▲ present data; □, Gracey, *et al.* (1951); ●, Merriam & Spaulding (1931); ▮▮, N.P.L. data (Pankhurst & Holder 1952).

Two tapered square-ended probes of a modified design were used in our experimental work. One, with $D_i/D = 0{\cdot}61$ at the tip, is shown in figure 13. The other, a similar probe with $D_i/D = 0{\cdot}64$, is described in our earlier paper (1969). The characteristics of these probes (see table 1 and figure 3) agree quite closely with those of square-nosed probes.

Effects of internal geometry

Consideration has been restricted to probes in which the impact hole is of constant diameter to a sufficient depth so that internal geometry is not a factor in probe performance. It is interesting, though, that some effects of internal geometry have been investigated by Gracey, Letko & Russell (1951), with a view to reducing the directional sensitivity relative to that of a square-nosed probe with the same tip D_i/D ratio. One variation was to introduce a conical bore in the mouth of a cylindrical probe, so that the internal passage converged from the full outside diameter D_o at the tip to $0{\cdot}1875\ D_o$ at some distance inside. Several other internal geometries were also examined, but the conclusions are generally the same: small decreases in directional sensitivity can be achieved, but the data depart from (5).

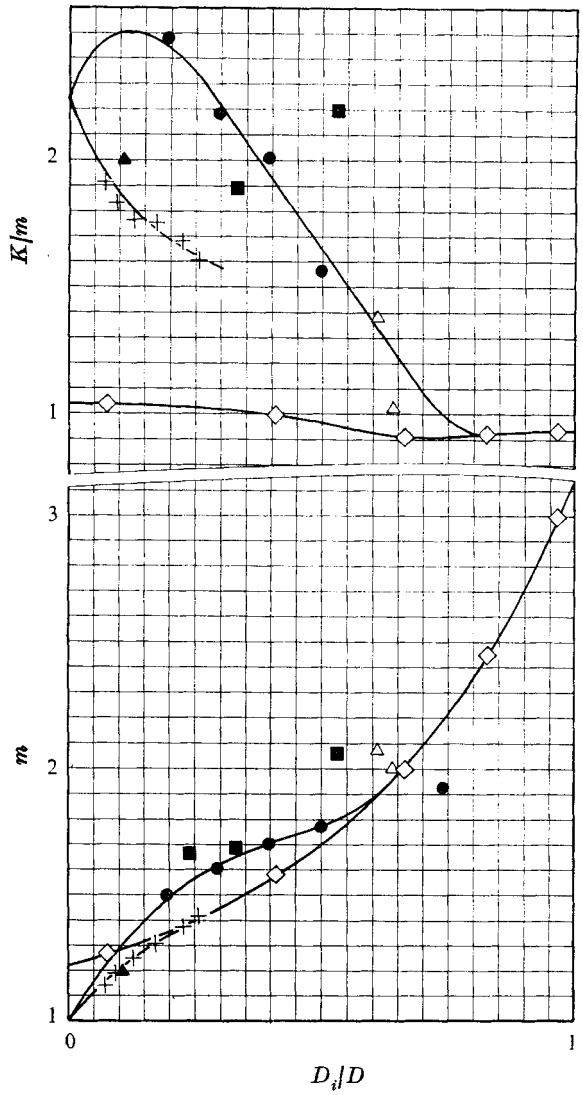

FIGURE 3. The parameters m and K/m as functions of D_i/D for sphere-nosed, round-nosed and square-nosed Pitot probes. Probe types: +, sphere-nosed; ◇, △, square-nosed; ●, ■, ▲, round-nosed. Data sources; +, △, ▲, present data; ◇, Davies (1957); ●, Merriam & Spaulding (1931); ■, N.P.L. data (Pankhurst & Holder 1952).

Effects of shrouding

Directional insensitivity exceeding that of the thin-walled tube can be achieved by placing a shroud (a short tube or venturi channel) around the tip of a simple probe, resulting in the device invented by Kiel (1935). Directional response data from a Kiel probe described by Pankhurst & Holder (1952, figure 92) follow (5), with $K = 25$ and $m = 15$. This high value of m confers virtually perfect total response up to $\theta = 45°$. Such a characteristic is not necessarily advantageous, however. The shroud also greatly increases the effective diameter of the probe, and adversely affects the transient response.

Probe geometry	Range	Relation	Maximum deviation, positive or negative
Sphere-nosed	$\lambda < 0{\cdot}26$	$K = \frac{9}{4}$, $m = 1+2{\cdot}35\lambda-3{\cdot}25\lambda^2$	4·5 %, 0·7 %
Round-nosed	$\lambda < 0{\cdot}35$	$K = \frac{9}{4}m$, $m = 1+3{\cdot}16\lambda-3{\cdot}6\lambda^2$	12 %, 1 %
Square-nosed	$0 < \lambda < 1$	$K = 0{\cdot}97m$, $m = 1+0{\cdot}225\exp(\frac{9}{4}\lambda)$	7 %, 0·7 %

TABLE 2. Empirical relations for the Pitot response parameters K and m as functions of the diameter ratio $\lambda \equiv D_i/D$

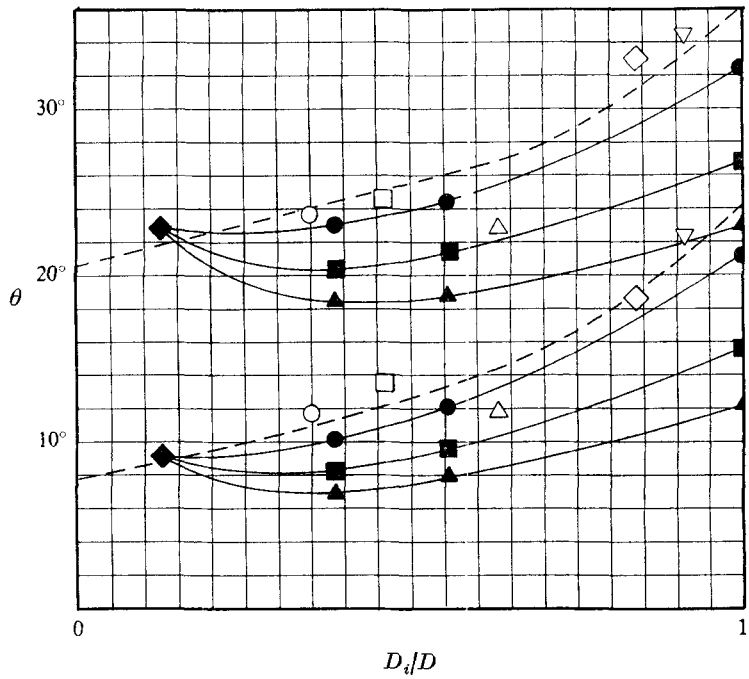

FIGURE 4. A comparison of response characteristics for tapered Pitot probes. Taper angles α: ○, ▽, 2·9°; ◇, 3·4°; □, 5°; ●, 7·5°; △, 13·6°; ■, 15°; ▲, 22·5°; ◆, any value (square-nosed probe, $D_i = D_o$). Ratios D_i/D_o: ●, ■, ◆, ▲, 0·125; ○, □, △, 0·20; ◇, 0·38. Data sources: ●, ■, ◆, ▲, Gracey *et al.* (1951); ○, □, ◇, △, the N.P.L., W.N.Y., B.S., and A.S.H.V.E. probes of Merriam & Spaulding (1931); ▽, the N.P.L. probes of Davies (1957). Top curves, $1-C = 0{\cdot}1$; bottom curves, $1-C = 0{\cdot}01$.

4. Effect of large-scale turbulence

Consider a Pitot probe in a statistically steady turbulent stream. Suppose that the probe is small relative to the local integral scale Λ of the turbulence and is oriented facing the mean velocity vector. Suppose also that the probe is internally blocked or constricted not far from the mouth, so that the fluid inside is essentially stagnant at equilibrium. We assume that the pressure P_s inside the

nose then follows the instantaneous velocity vector as in a steady uniform laminar stream:

$$P_s = P + \tfrac{1}{2}C\rho U^2 = P + \tfrac{1}{2}\rho U^2[1 - K(\sin^2\theta)^m]$$
$$= P + \tfrac{1}{2}\rho U^2[1 - K(U_n^2/U^2)^m]. \tag{6}$$

When P_s is time averaged,

$$\overline{P}_s = \overline{P} + \tfrac{1}{2}\rho\overline{U^2} - \tfrac{1}{2}K\rho\overline{U^{2(1-m)}U_n^{2m}}. \tag{7}$$

Since the probe is considered to be parallel to the mean velocity vector $\overline{\mathbf{U}}$, we have $U_y = U_z = 0$ and $U_n^2 = U_y^2 + U_z^2 = u_y^2 + u_z^2$, where u_y and u_z are the fluctuating components of U_y and U_z.

The key parameter in (7) is the exponent m. The minimum value, $m = 1$, gives linear response to the mean-square transverse velocity fluctuation

$$\overline{U_n^2} = \overline{u_y^2} + \overline{u_z^2};$$
$$\overline{P}_s = \overline{P} + \tfrac{1}{2}\rho\overline{U^2} - \tfrac{1}{2}K\rho\overline{U_n^2}. \tag{8}$$

The maximum value for simple probes, $m = 3{\cdot}1$, makes the transverse response negligible over a usefully broad range of U_n^2/U^2, in which case

$$\overline{P}_s = \overline{P} + \tfrac{1}{2}\rho\overline{U^2}. \tag{9}$$

A special case occurs when the turbulence level is very low; then $\overline{U_n^2}$, $\overline{u_x^2} \ll \overline{U}_x^2$, giving

$$\overline{P}_s = \overline{P} + \tfrac{1}{2}\rho\overline{U^2} - \tfrac{1}{2}K\rho(\overline{U}_x^2)^{1-m}\overline{U_n^{2m}}. \tag{10}$$

The theory of the general case is developed through the statistical interpretation of the quantity $\overline{U^{2(1-m)}U_n^{2m}}$. We have $U_n^2 = u_y^2 + u_z^2$ and $U^2 = \overline{U}_x^2 + u_x^2 + u_y^2 + u_z^2$. Thus

$$\overline{U^{2(1-m)}U_n^{2m}} = \int_{-\infty}^{\infty}\int_{-\infty}^{\infty}\int_{-\infty}^{\infty} g f_{xyz}\,du_x\,du_y\,du_z, \tag{11}$$

where $f_{xyz}(u_x, u_y, u_z)$ is the joint probability function of u_x, u_y and u_z, and

$$g(\overline{U}_x, u_x, u_y, u_z) \equiv U^{2(1-m)}U_n^{2m} = (\overline{U}_x^2 + u_x^2 + u_y^2 + u_z^2)^{1-m}(u_y^2 + u_z^2)^m.$$

A useful first approximation to the value of the definite triple integral is obtained by supposing the following.

(i) The velocity fluctuations are uncorrelated, giving

$$f_{xyz}(u_x, u_y, u_z) = f_x(u_x)f_y(u_z)f_z(u_z).$$

(ii) The velocity fluctuations are normally distributed, so that

$$f_x(u_x) = [\hat{u}_x(2\pi)^{\frac{1}{2}}]^{-1}\exp(-u_x^2/2\overline{u_x^2})$$

with analogous relations for u_y and u_z, where $\hat{u}_x \equiv (\overline{u_x^2})^{\frac{1}{2}}$, etc.

(iii) The variances of the velocity fluctuations have a constant relation, say

$$\overline{u_y^2} = \overline{u_z^2}, \quad \overline{u_x^2} = \beta\overline{U_n^2},$$

where $\overline{u_y^2} + \overline{u_z^2} = \overline{U_n^2}$ and β is a constant. In isotropic turbulence $\beta = \frac{1}{2}$, while in turbulent shear flows $\beta = 1$ is a better approximation.

The solution of (11) under the stated conditions is of the general form

$$\overline{U^{2(1-m)}U_n^{2m}} = \overline{U}_x^2 v^{2m}\psi(m,\beta,v^2), \tag{12}$$

where $v^2 \equiv \overline{U_n^2}/\overline{U}_x^2$ and ψ is the value of the normalized (non-dimensional) definite triple integral. Because of cylindrical symmetry, it is possible to replace the rectangular surface element $du_y du_z$ by a ring $2\pi U_n dU_n = \pi dU_n^2$ and thus reduce the integral to two dimensions, giving

$$\psi = \frac{2}{\sqrt{\pi}}\int_0^\infty \int_0^\infty [1+v^2(\eta+2\beta\xi^2)]^{1-m}\eta^m e^{-\eta}e^{-\xi^2}d\xi\,d\eta, \tag{13}$$

where $\xi^2 \equiv u_x^2/2\overline{u_x^2}$ and $\eta \equiv U_n^2/\overline{U_n^2}$. This result is analytic in the limit $\psi \to \psi_0$ as $v^2 \to 0$, yielding the gamma function $\psi_0 = \Gamma(m+1)$ in general, and $\psi_0 = m!$ for integer values of m in particular.

The range of $v^2 \equiv \overline{U_n^2}/\overline{U}_x^2$ is $0 < v^2 < \infty$, whereas that of $w^2 \equiv \overline{U_n^2}/\overline{U^2}$ is $0 \leqslant w^2 < (1+\beta)^{-1}$, where

$$w^2 = v^2/[1+(1+\beta)v^2]. \tag{14}$$

Furthermore, when v^2 is large, the uncertainty in experimental values of $\overline{U}_x^2$ may be great. It is thus advantageous to write (12) in the modified form

$$\overline{U^{2(1-m)}U_n^{2m}} = \overline{U^2}w^{2m}\chi\Gamma(m+1), \tag{15}$$

where $$\chi \equiv (\overline{U}_x^2/\overline{U^2})^{1-m}\psi/\psi_0 = [1+(1+\beta)v^2]^{m-1}\psi/\Gamma(m+1).$$

The function χ has been computed for

$$\beta = \tfrac{1}{2}, \tfrac{3}{4}, 1, \tfrac{3}{2}, 2, \quad m = 1, 1{\cdot}02, 1{\cdot}05, 1{\cdot}1, 1{\cdot}2, 1{\cdot}4, \ldots, 3{\cdot}0, 3{\cdot}2,$$
$$w^2 = 0{\cdot}01, 0{\cdot}02, 0{\cdot}03, 0{\cdot}05, 0{\cdot}07, 0{\cdot}1, 0{\cdot}15, 0{\cdot}2, 0{\cdot}3, \ldots .$$

The numerical output, consisting of tables of χ and $1-\chi$, is available in a report (Becker & Brown 1972) and a sample is shown in table 3. The data are well fitted by

$$\chi = 1 - Aw^2/(1+Bw^2), \tag{16}$$

$$A = A_1 + A_2(m-1)^a, \quad B = B_1 + B_2/(m-1), \tag{17), (18}$$

where A_1, A_2, B_1, B_2 and a are defined in table 4. The predicted values of χ are accurate to within $\pm 0{\cdot}5\,\%$ when $w^2 < 0{\cdot}3$ and to within $\pm 0{\cdot}1\,\%$ in major portions of this region. The equations are thus of comparable accuracy with ordinary Pitot probe measurements, and should be satisfactory for most purposes.

5. Total Pitot response

The quantity actually measured by a Pitot probe operated as described at the beginning of §4 is

$$\overline{P}_s - P^0 - \overline{P} - P^0 + \tfrac{1}{2}\rho\overline{U^2} - \tfrac{1}{2}K\rho\overline{U^{2(1-m)}U_n^{2m}}, \tag{19}$$

where P^0 is a reference pressure. We shall consider two interesting cases: (i) $P^0 = \overline{P}$ and (ii) $P^0 = P_b$, where P_b is the mean static pressure at the boundary of a turbulent flow that satisfies the boundary-layer approximations.

w_2	0·01	0·02	0·05	0·10	0·20	$\frac{2}{3}$
v^2	0·0101	0·0206	0·0540	0·1176	0·2857	∞
m	χ	χ	χ	χ	χ	χ
1·05	0·9952	0·9947	0·9933	0·9912	0·9878	0·9799
1·2	0·9952	0·9930	0·9867	0·9775	0·9626	0·9279
1·6	0·9903	0·9814	0·9578	0·9236	0·8724	0·7696
2·0	0·9807	0·9627	0·9152	0·8519	0·7616	0·5990
2·4	0·9680	0·9386	0·8637	0·7690	0·6434	0·4419
2·8	0·9525	0·9100	0·8053	0·6805	0·5277	0·3111
3·2	0·9345	0·8773	0·7421	0·5912	0·4212	0·2100

(*a*)

w^2	0·01	0·02	0·05	0·10	0·20	$\frac{1}{2}$
v^2	0·0102	0·0208	0·0555	0·1250	0·3333	∞
m	χ	χ	χ	χ	χ	χ
1·05	0·9952	0·9947	0·9933	0·9915	0·9886	0·9860
1·2	0·9953	0·9930	0·9870	0·9786	0·9663	0·9550
1·6	0·9903	0·9817	0·9586	0·9277	0·8843	0·8450
2·0	0·9808	0·9632	0·9177	0·8591	0·7810	0·7114
2·4	0·9862	0·9394	0·8674	0·7792	0·6685	0·5725
2·8	0·9528	0·9111	0·8102	0·6933	0·5559	0·4423
3.2	0·9349	0·8788	0·7482	0·6057	0·4503	0·3290

(*b*)

TABLE 3. Values of the Pitot response function χ for flows with (*a*) $\beta = \frac{1}{2}$ and (*b*) $\beta = 1$

Range of m	A_1	A_2	a
$\leqslant 2{\cdot}5$	0·1806	1·810	1·674
$\geqslant 2{\cdot}5$	0	1·880	1·667

β	Range of m	B_1	B_2
$\frac{1}{2}$	$\leqslant 2{\cdot}5$	2·833	0·5278
$\frac{1}{2}$	$\geqslant 2{\cdot}5$	2·833	$0{\cdot}5278 + 0{\cdot}000069\,e^{2{\cdot}87m}$
1	$\leqslant 2{\cdot}5$	3·13	0·965
1	$\geqslant 2{\cdot}5$	3·50	0

TABLE 4

The case $P^0 = \bar{P}$

This is the case of a Pitot-static (combined impact and static pressure) probe with ideal static pressure response. The degree to which such a response is realizable is unclear, and a critical study of static pressure probes designed for use in turbulent flows is needed to resolve the question.

We define a pair of functions to measure departures from the two most interesting standards of performance, (i) the direct detection of $\frac{1}{2}\rho\overline{U^2}$ and (ii) the direct detection of $\frac{1}{2}\rho\bar{U}_x^2$:

$$F \equiv 1-(\bar{P}_s-\bar{P})/\tfrac{1}{2}\rho\overline{U^2}, \quad F_x \equiv 1-(\bar{P}_s-\bar{P})/\tfrac{1}{2}\rho\bar{U}_x^2. \qquad (20), (21)$$

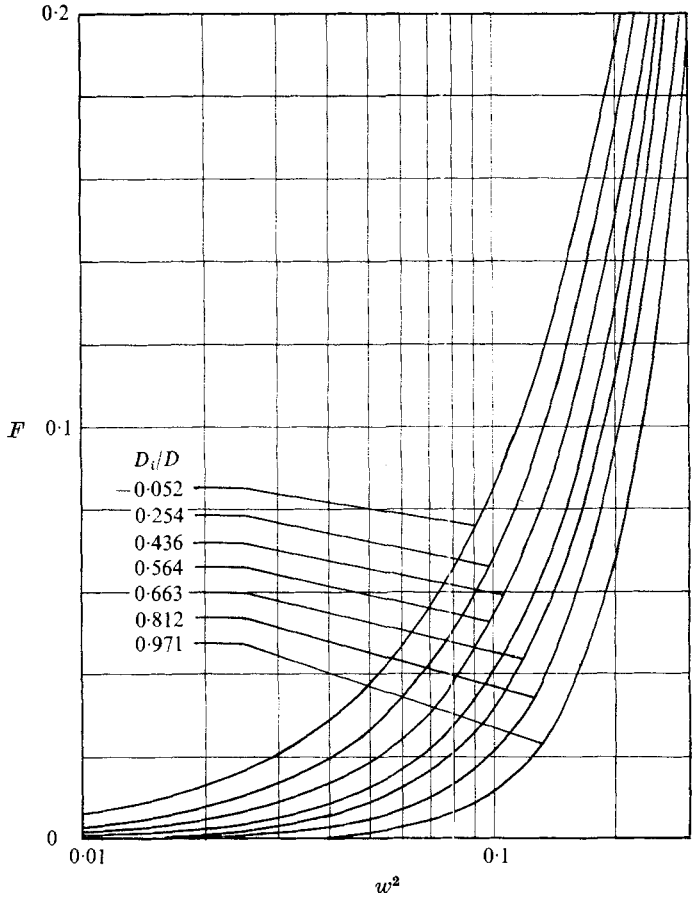

FIGURE 5. The function F for square-nosed probes in flows with $\beta = 1$. The values of D_i/D, given (from table 2) by $D_i/D = \frac{4}{9}\ln[4{\cdot}44\,(m-1)]$, correspond to $m = 1{\cdot}2$, $1{\cdot}4$, $1{\cdot}6$, $1{\cdot}8$, $2{\cdot}0$, $2{\cdot}4$, $3{\cdot}0$. The value $D_i/D = -0{\cdot}052$ is artificial.

From the results in the preceding section

$$F = Kw^{2m}\chi\Gamma(m+1), \quad F_x = 1-(1-F)/[1-(1+\beta)w^2]. \qquad (22), (23)$$

These functions have been computed for $\beta = \frac{1}{2}$ and 1 and for values of m and K appropriate to square-nosed, round-nosed and sphere-nosed probes (Becker & Brown 1972). Examples of the results are shown in figures 5 and 6. F is always positive, whereas F_x can be positive or negative.

The selection of probes whose response approximates one of the standards is facilitated by graphs of w^2 *vs.* D_i/D at fixed values of F and F_x. Values of $\pm 0{\cdot}01$ and $\pm 0{\cdot}03$ are suitable, representing interesting levels of error in the detection of $\frac{1}{2}\rho\overline{U^2}$ and $\frac{1}{2}\rho\overline{U}_x^2$. The following conclusions are indicated.

(i) The quantity $\frac{1}{2}\rho\overline{U^2}$ is most accurately defined by square-nosed probes of large D_i/D ratio. These, in other words, give small values of F over a much broader range of turbulence levels w^2 than do round-nosed or sphere-nosed probes. The effect of D_i/D is shown in figure 7.

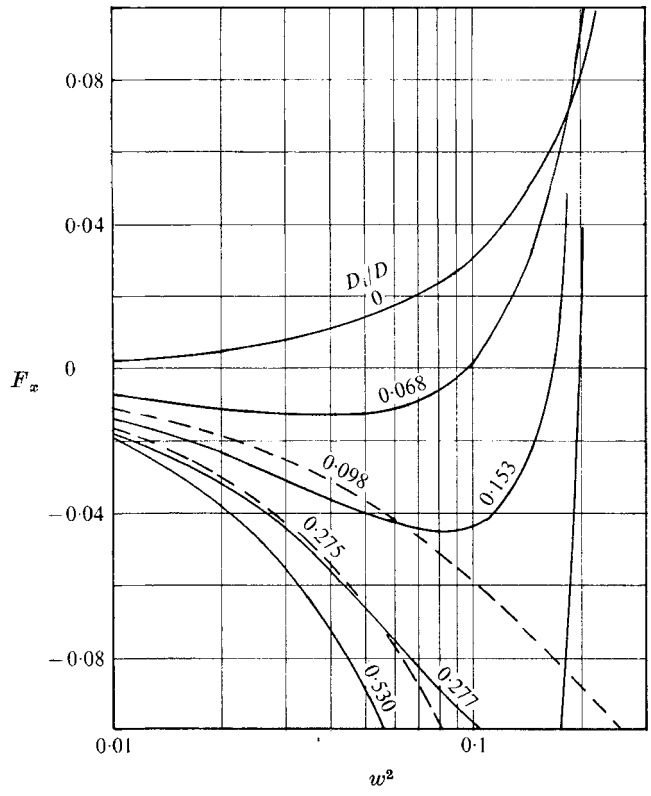

FIGURE 6. The function F_x for round-nosed (full curves) and sphere-nosed (dashed curves) probes in flows with $\beta = 1$.

β	$\frac{1}{2}$	1	$\frac{1}{2}$	1
Range of F_x	$\pm 0{\cdot}03$	$\pm 0{\cdot}03$	$\pm 0{\cdot}01$	$\pm 0{\cdot}01$
Optimum D_i/D	0·24	0·12	0·125	0·05
Range of w^2	$\leqslant 0{\cdot}15$	$\leqslant 0{\cdot}17$	$\leqslant 0{\cdot}075$	$\leqslant 0{\cdot}09$

TABLE 5

(ii) The quantity $\frac{1}{2}\rho\overline{U}_x^2$ is most accurately defined by round-nosed probes with $D_i/D < 0{\cdot}3$. The effect of D_i/D on F_x is shown in figure 8. At $w^2 < 0{\cdot}1$, $|F_x| < 0{\cdot}03$ in the range $0{\cdot}12 < D_i/D < 0{\cdot}24$ when $\beta = \frac{1}{2}$ and $0 < D_i/D < 0{\cdot}12$ when $\beta = 1$. At the optimum value of D_i/D, the range of w^2 in which F_x is smaller than a given value is maximal; see table 5. Since $\frac{1}{2} < \beta < 1$ in most flows of interest, the overall optimum may be taken to be $D_i/D \simeq 0{\cdot}12$.

(iii) Sphere-nosed probes behave sufficiently like round-nosed probes to be practically indistinguishable from them.

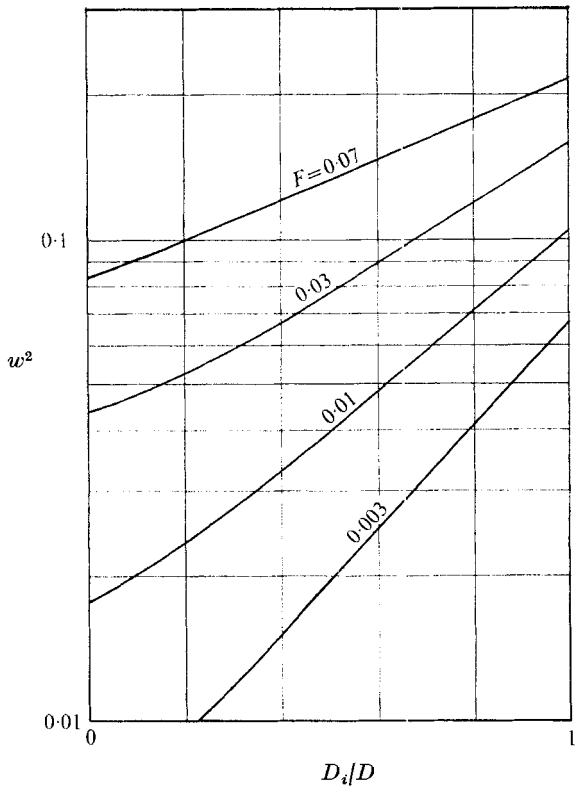

FIGURE 7. The turbulence level w^2 at which the function F takes the values 0·003, 0·01, 0·03 and 0·07 as a function of D_i/D for square-nosed probes in flows with $\beta = 1$. Results for $\beta = \frac{1}{2}$ are virtually the same.

The case $P^0 = P_b$

In a turbulent flow that satisfies the classical thin-boundary-layer assumptions (boundary layers, duct flows, jets, wakes and mixing layers), the lateral component of the equation of motion reduces to

$$P_b - \overline{P} = \rho \overline{u_v^2}, \tag{24}$$

for planosymmetric flows, and

$$P_b - \overline{P} = \rho \overline{u_r^2} + \int_r^b \frac{\overline{u_\phi^2} - \overline{u_r^2}}{r}\, dr \tag{25}$$

for axisymmetric flows, where $y = b$ or $r = b$ at the shear-layer edge (the wall in a boundary layer or duct flow, or just inside the free stream in a jet, wake or mixing layer), $\overline{P}$ is the local mean static pressure and $\overline{P} \equiv P_b$ at $r = b$. We assume that, to a good approximation, $\overline{u_y^2} = \overline{u_z^2}$ or $\overline{u_r^2} = \overline{u_\phi^2}$. Then, in the present context,

$$P_b - \overline{P} \simeq \tfrac{1}{2}\rho \overline{U_n^2}. \tag{26}$$

Reasonably accurate detection of P_b is usually not difficult. The measurement of $\overline{P}_s - P_b$ is then the most effective way to use a Pitot probe in such flows.

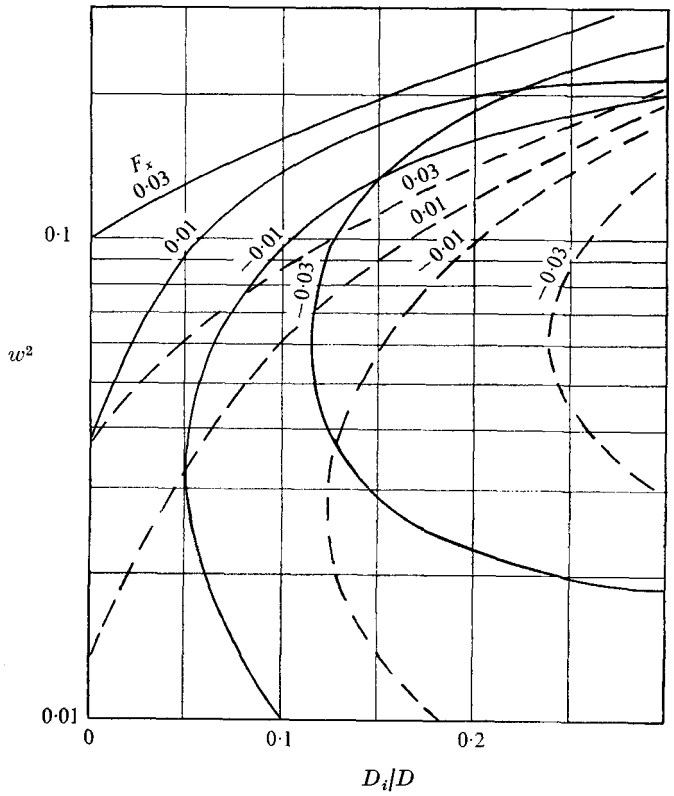

FIGURE 8. The turbulence level w^2 at which the function F_x takes the values $-0{\cdot}03$, $-0{\cdot}01$, $0{\cdot}01$ and $0{\cdot}03$ as a function of D_i/D for round-nosed probes in flows with $\beta = \frac{1}{2}$ (dashed curves) and $\beta = 1$ (full curves).

β	$\frac{1}{2}$	1	$\frac{1}{2}$	1
Range of G_x	$\pm 0{\cdot}03$	$\pm 0{\cdot}03$	$\pm 0{\cdot}01$	$\pm 0{\cdot}01$
Optimum D_i/D	$> 0{\cdot}47$	$0{\cdot}45$	$0{\cdot}59$	$0{\cdot}24$
Range of w^2	—	$\leqslant 0{\cdot}16$	$\leqslant 0{\cdot}11$	$\leqslant 0{\cdot}075$

TABLE 6

The same approach as in the case $P^0 = \bar{P}$ can be employed. We define

$$G \equiv 1-(\bar{P}_s-P_b)/\tfrac{1}{2}\rho\overline{U^2}, \quad G_x \equiv 1-(\bar{P}_s-P_b)/\tfrac{1}{2}\rho\bar{U}_x^2, \qquad (27), (28)$$

and obtain

$$G = F+w^2, \quad G_x = F_x+v^2. \qquad (29), (30)$$

Values of G and G_x have been computed together with those of F and F_x (Becker & Brown 1972). The graphs of G and G_x *vs.* w^2 are qualitatively similar to those of F and F_x, shown in figures 5 and 6.

Graphs of w^2 *vs.* D_i/D at fixed values of G and G_x indicate the following conclusions.

(i) There is no probe that responds with reasonable accuracy to $\frac{1}{2}\rho\overline{U^2}$, i.e. at no value of D_i/D is the value of G small over a broad range of w^2.

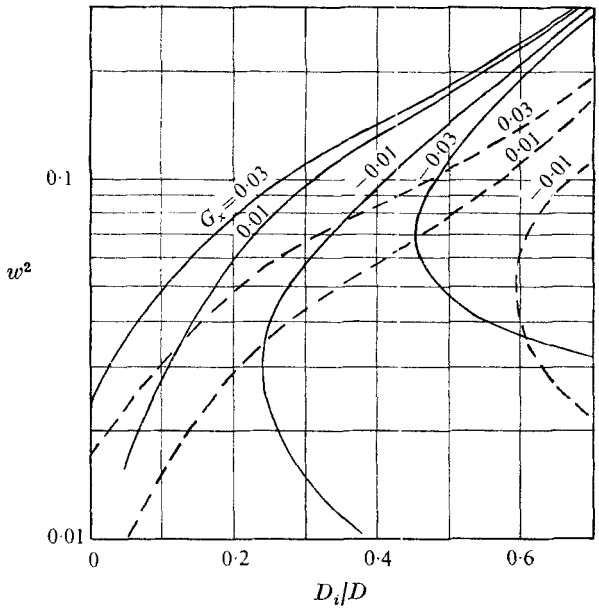

FIGURE 9. The turbulence level w^2 at which the function G_x takes the values $-0{\cdot}03$, $-0{\cdot}01$, $0{\cdot}01$ and $0{\cdot}03$ as a function of D_i/D for round-nosed probes in flows with $\beta = \frac{1}{2}$ (dashed curves) and $\beta = 1$ (full curves).

(ii) Round-nosed probes can be used to detect $\frac{1}{2}\rho\overline{U}_x^2$ with good accuracy. Figure 9 indicates that at $w^2 < 0{\cdot}1$, $|G_x| < 0{\cdot}03$ in the range $D_i/D > 0{\cdot}47$ when $\beta = \frac{1}{2}$ and $0{\cdot}27 < D_i/D < 0{\cdot}45$ when $\beta = 1$. At the optimum value of D_i/D for given limits of G_x the range of w^2 is maximal, see table 6. The overall optimum value of D_i/D is about $0{\cdot}45$.

(iii) Square-nosed probes can also detect $\frac{1}{2}\rho\overline{U}_x^2$ with reasonable accuracy. Figure 10 indicates that for $w^2 < 0{\cdot}1$, $|G_x| < 0{\cdot}03$ in the range $0{\cdot}14 < D_i/D < 0{\cdot}74$ when $\beta = \frac{1}{2}$ and $0{\cdot}14 < D_i/D < 0{\cdot}15$ when $\beta = 1$. The overall optimum D_i/D is roughly $0{\cdot}15$.

(iv) Sphere-nosed probes behave rather like round-nosed probes in the detection of $\frac{1}{2}\rho\overline{U}_x^2$, but are slightly less accurate.

6. Differential Pitot response

Consider measurements made at the same point in a turbulent flow, or at statistically equivalent points, with two probes having different values of the transverse response parameters m and K. The difference $\Delta\overline{P}_s \equiv \overline{P}_{s1} - \overline{P}_{s2}$ in the time-averaged responses is

$$\Delta\overline{P}_s = H_2 - H_1, \tag{31}$$

where

$$H = \tfrac{1}{2}\rho\overline{U^2}Kw^{2m}\chi\Gamma(m+1) \equiv \tfrac{1}{2}\rho\overline{U}_x^2 Kv^{2m}[1+(1+\beta)v^2]^{1-m}\chi\Gamma(m+1).$$

In terms of the functions defined in the preceding section,

$$\begin{aligned}\Delta\overline{P}_s &= \tfrac{1}{2}\rho\overline{U^2}(F_2 - F_1) = \tfrac{1}{2}\rho\overline{U^2}(G_2 - G_1)\\ &= \tfrac{1}{2}\rho\overline{U}_x^2(F_{x2} - F_{x1}) = \tfrac{1}{2}\rho\overline{U}_x^2(G_{x2} - G_{x1}).\end{aligned} \tag{32}$$

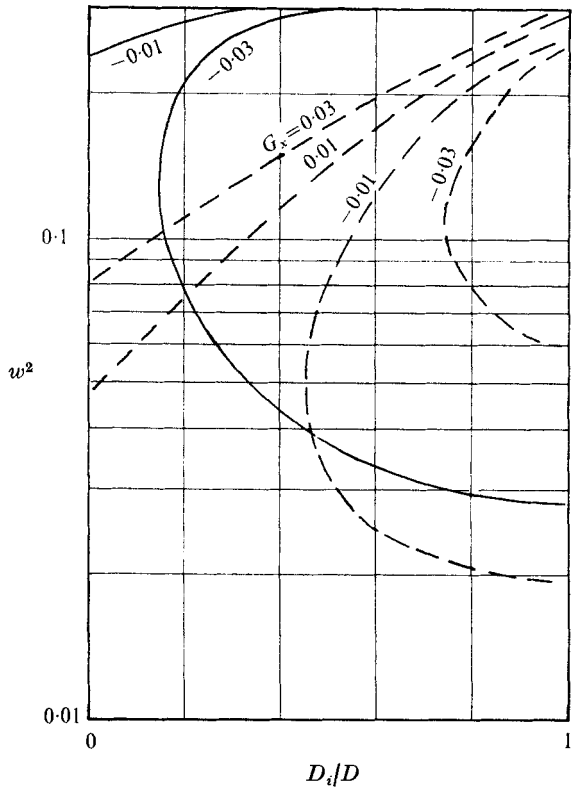

FIGURE 10. The turbulence level w^2 at which the function G_x takes the values $-0{\cdot}03$, $-0{\cdot}01$, $0{\cdot}01$ and $0{\cdot}03$ as a function of D_i/D for square-nosed probes in flows with $\beta = \frac{1}{2}$ (dashed curves) and $\beta = 1$ (full curves).

These relations can be used for the measurement of the mean-square transverse velocity fluctuation $\overline{U_n^2} \equiv w^2\overline{U^2} \equiv v^2\overline{U}_x^2$. A useful alternative form is obtained by normalizing (32) by the response of one of the probes. If the flow is a turbulent shear flow satisfying the thin-boundary-layer assumptions, and if the reference pressure P^0 is taken at the shear-layer edge, $P^0 = P_b$, then

$$\frac{\Delta\bar{P}_s}{\bar{P}_{si}-P_b} = \frac{F_2-F_1}{1-\overline{w^2}-F_i} = \frac{G_2-G_1}{1-G_i} = \frac{G_{x2}-G_{x1}}{1-G_{xi}}, \tag{33}$$

where $i = 1$ or 2.

Experimental results for square-nosed probes

The practical application of (32) and (33) is illustrated by a set of unpublished results obtained during an earlier, unrelated investigation. Impact pressure profiles were measured at a section 18 nozzle diameters downstream in a confined, turbulent, round air jet. The jet facility is described elsewhere (Becker, Hottel & Williams 1963). The value of the confined-jet performance parameter, the Craya–Curtet number Ct (Becker *et al.* 1963), was 0·345, and the flow in the region of interest was virtually indistinguishable from a free jet discharging into a body of still air (negligible free-stream velocity, virtually zero axial pressure gradient). The nozzle diameter was 0·635 cm and the nozzle air velocity was 130 m/s. The

	D_o (mm)	D_i (mm)	D (mm)	D_i/D	m	K
Probe A	0·89	0·59	0·59	1·00	3·1	2·9
Probe B	0·56	0·31	0·56	0·55	1·8	1·0

TABLE 7

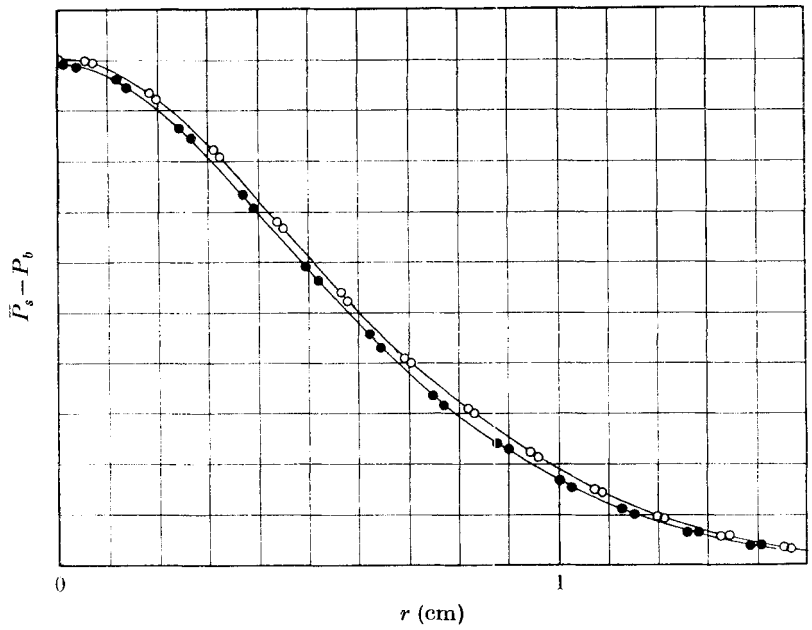

FIGURE 11. Impact pressure profiles in a round air jet at $x/D_j = 18$, measured with two square-nosed Pitot probes with different diameter ratios. ○, $D_i/D \approx 1$; ●, $D_i/D = 0{\cdot}55$.

two Pitot probes were made of stainless-steel hypodermic tubing. One, A, was sharp-lipped and the other, B, was square-nosed. The salient characteristics are given in table 7. The directional response was not studied experimentally, and the values of m and K have therefore been estimated from figure 3. The reference pressure P^0 was taken from a static pressure tap in the wall of the confining duct, and should be virtually the same as the mean static pressure P_b at the jet edge.

The impact pressure profiles measured at $x/D_j = 18$, where x is downstream distance and D_j the nozzle diameter, are shown in figure 11. The integral scale of the turbulence was approximately $\Lambda = 6$ mm (Becker, Hottel & Williams 1967, figure 12). Thus the condition in the present theory of Pitot response, that the turbulence scale be large compared with the probe diameter, should be satisfied. The near equality of the characteristic diameters D should ensure that the effect of the mean velocity gradient (the displacement effect) tends to vanish in the differential response. The probe was well damped (15 s time constant for 50 % change), and the accuracy of the manometer readings was $\pm$ 0·1 % or better. In view of these considerations, the data should be adequate for accurate calculations from (33).

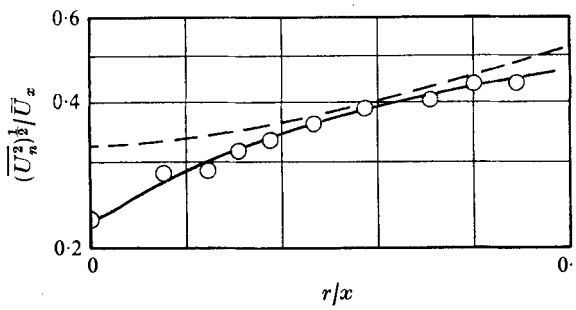

FIGURE 12. Turbulence intensity profile in a round air jet. ○, from present measurements with two square-nosed Pitot probes, at $x/D_j = 18$; – –, hot-wire results of Wygnanski & Fielder (1969), at $x/D_j = 60$.

The results, figure 12, show that the profile of the total relative intensity of transverse velocity fluctuations, $\overline{U_n^2})^{\frac{1}{2}}/\overline{U}_x$, is of the form expected from past studies of free round jets with hot-wire anemometers (e.g. Corrsin & Uberoi 1950; Gibson 1963; Wygnanski & Fiedler 1969). The data of Wygnanski & Fiedler for $x/D_j = 60$, the smallest x/D_j at which radial profiles were obtained, are shown for comparison. The hot-wire results around the jet centre-line are significantly higher than the present data, but this simply reflects the growth of the relative intensity with x/D_j towards the self-preserving distribution which is closely approached in free jets around $x/D_j = 100$. At $r/x > 0{\cdot}04$ the two profiles are close together, in accord with the fact that self-preservation is approached most rapidly in the region of maximum shear. The relative intensity 0·23 on the jet centre-line agrees with the results obtained on a much larger jet with another pair of Pitot probes; see figure 15.

The above results are of special interest because (i) the probes were near the minimum practical size, (ii) the characteristic probe diameters were matched to minimize the influence of the displacement effect in a velocity gradient, (iii) the differences in the directional characteristics of the probes were not great, but the differential response was still quite accurately measurable, and (iv) the transverse dimensions of the flow, approximately 1 cm radius to the velocity half-amplitude point, were not far from the minimum below which accurate measurements would be very difficult with even the smallest practical probes.

Results for a differential Pitot probe

Since turbulence detection requires two Pitot probes with different directional characteristics, it is convenient, when the flow to be studied is adequately large, to couple the probes rigidly in one instrument. The differential response can then be measured directly. The two probe tips must, of course, be at statistically equivalent points in the flow (virtually equal mean velocity, mean static pressure and mean turbulence properties). In axisymmetric or planosymmetric flows, traversing can be arranged so that the tip distances from the flow centre are equal.

We have previously described an instrument in which a square-nosed probe was coupled with a sphere-nosed probe (Becker & Brown 1969). The name

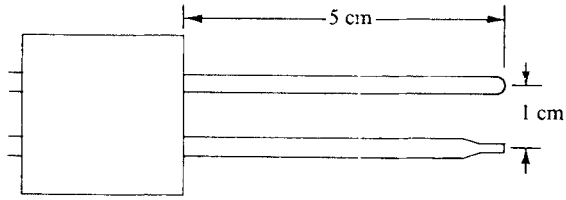

FIGURE 13. Differential Pitot probe. The support block is a 2·5 cm square by 0·62 cm thick block, rounded on the leading edge. The square-tipped component probe is of 3·17 mm O.D. by 1·37 mm I.D. tubing, tapered at 15° to 1·37 mm O.D. over the final 4 mm of its length. The round-nosed component probe is of 3·17 mm tubing with a solid insert at the tip, drilled with a 0·34 mm diameter hole. Material was type 310 stainless steel, for high-temperature service.

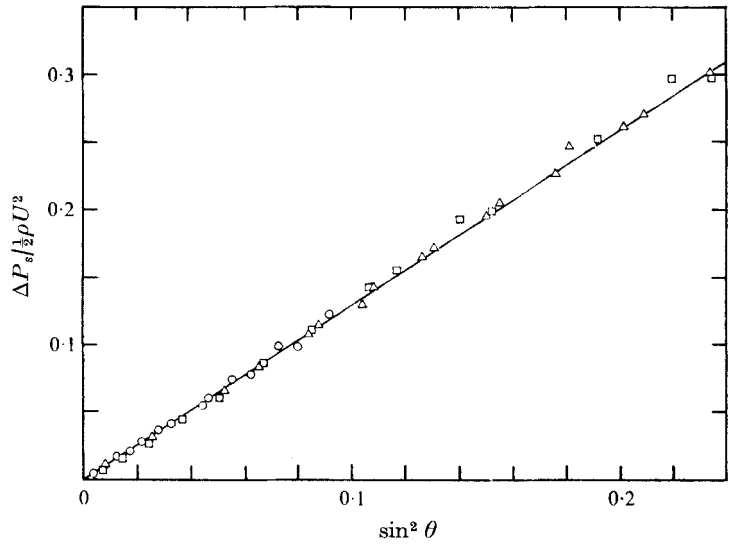

FIGURE 14. Differential response characteristics of the differential Pitot probe, at various Reynolds numbers. *Re* values: ○, 3800; □, 6200; △, 11500.

'differential Pitot probe' was given to such devices in general. The probe was used for turbulence measurements in air jets and flames, but the interpretation of the data was simplistic in light of the present theory. We have subsequently built another probe of this type, very rugged and suitable for use in flames, and have tested it by making turbulence measurements in a large free air jet. The probe (figure 13) consisted of a 3·18 mm diameter round-nosed tube, $D_i/D = 0{\cdot}108$, coupled with a 1·37 mm tip diameter square-tipped, tapered (but effectively square-nosed) tube, $D_i/D = 0{\cdot}61$. The directional response characteristics, determined in a uniform wind-tunnel stream (Brown 1971), were $m = 1{\cdot}192$ and $K = 2{\cdot}39$ for the round-nosed leg and $m = 2{\cdot}13$ and $K = 2{\cdot}49$ for the square-nosed leg (data are also shown in table 1 and figures 1, 2 and 3). Tests at various wind velocities indicated no effect of Reynolds number in the range of present interest ($Re > 3000$, *Re* based on diameter of round-nosed leg). The differential response (figure 14) was virtually linear in $\sin^2\theta = U_n^2/U^2$, giving

$$\Delta P_s = 1{\cdot}29(\tfrac{1}{2}\rho U_n^2). \tag{34}$$

$w^2 = \overline{U_n^2}/\overline{U^2}$	$v^2 \equiv \overline{U_n^2}/\overline{U_x^2}$		$\dfrac{F_2-F_1}{w^2} \equiv \dfrac{\Delta\bar{P}_s}{\frac{1}{2}\rho\overline{U_n^2}}$		$\dfrac{F_2-F_1}{v^2(1-F_1-w^2)} \equiv \dfrac{\overline{U_x^2}}{\overline{U_n^2}}\dfrac{\Delta\bar{P}_s}{\bar{P}_s-P_b}$	
	$\beta = \frac{1}{2}$	$\beta = 1$	$\beta = \frac{1}{2}$	$\beta = 1$	$\beta = \frac{1}{2}$	$\beta = 1$
0·01	0·0101	0·0102	1·042	1·042	1·036	1·030
0·02	0·0206	0·0208	1·152	1·152	1·142	1·130
0·03	0·0314	0·0319	1·207	1·207	1·192	1·173
0·05	0·0545	0·0556	1·253	1·253	1·233	1·200
0·07	0·0782	0·0814	1·261	1·259	1·240	1·190
0·10	0·1176	0·1250	1·241	1·239	1·228	1·150
0·15	0·1935	0·2143	1·168	1·160	1·192	1·071
0·2	0·2857	0·3333	1·075	1·059	1·169	0·993
0·3	0·5455	0·7500	0·866	0·816	1·305	0·945

TABLE 8. Response functions for the differential Pitot probe shown in figure 13, coupling a square-nosed component probe ($m = 2{\cdot}13$, $K = 2{\cdot}94$, subscript 1) with a round-nosed one ($m = 1{\cdot}192$, $K = 2{\cdot}39$, subscript 2)

The fact that differential probes with this characteristic are possible was also observed in our earlier work (Becker & Brown 1969). These probes provide a particularly simple device for detecting the transverse component of the stream velocity.

The performance in a turbulent flow, with the probe oriented into the mean velocity vector, has been computed from (33) for β values of $\frac{1}{2}$ and 1. The results (table 8) can be compared with the hypothetical case of a probe with the same values of m and K, but of such a size that the distance L, separating the component probes, is small relative to the turbulence scale Λ. Consider the time mean of the difference in instantaneous pressure signals received by the component probes. Equation (34) gives

$$\overline{\Delta P_s} = 1{\cdot}29(\tfrac{1}{2}\rho\overline{U_n^2}), \tag{35}$$

if $L \ll \Lambda$. A significant feature of the differential response $\Delta\bar{P}_s$ of the actual probe is thus seen to be that it approximates this $\overline{\Delta P_s}$; i.e.

$$\Delta\bar{P}_s|_{\text{actual}} \simeq \lim_{L\to 0} \overline{\Delta P_s}. \tag{36}$$

Such a relation was postulated earlier for a similar probe (Becker & Brown 1969), and has now been shown to be reasonably close to the truth.

Equation (36) has useful corollary. Consider a situation where the differential Pitot probe is at an angle to the mean velocity vector. The differential response approximates

$$\Delta\bar{P}_s = 1{\cdot}29(\tfrac{1}{2}\rho\overline{U_n^2}), \tag{37}$$

where, now, $\overline{U_n^2} = \bar{U}_y^2 + \bar{U}_z^2 + \overline{u_y^2} + \overline{u_z^2}$. Another feature of interest (table 8) is the near constancy of the normalized response in the form $(\bar{U}_x^2/\overline{U_n^2})[\Delta\bar{P}_s/(\bar{P}_{s1}-P_b)]$, where subscript 1 indicates the square-nosed component probe. We obtain

$$\Delta\bar{P}_s/(\bar{P}_{s1}-\bar{P}_b) = 1{\cdot}15\overline{U_n^2}/\bar{U}_x^2. \tag{38}$$

It remains to describe the experiment in which the probe was used for the detection of turbulence in a free air jet. The jet nozzle diameter D_j was 7·5 cm and the nozzle air velocity was 55 m/s. Measurements were made along the jet axis over the range $6 \leqslant x/D_j \leqslant 90$, where x is downstream distance. The integral scale of the turbulence can be estimated from a formula based on results of Wygnanski & Fiedler (1969): $\Lambda \simeq 0{\cdot}04x$. The relative integral scale Λ/D varied between 6 at $x/D_j = 6$ and 90 at $x/D_j = 90$, where D is the diameter of the round-nosed component Pitot probe (the larger of the two components). Thus the condition $\Lambda \gg D$, for quasi-steady quasi-laminar instantaneous signal development, was fairly well satisfied. The probe straddled the jet centre-line. The jet was however so large, laterally, that conditions at the probe tips were virtually the same as on the centre-line, and transverse gradients in the mean velocity were insignificant. On the jet centre-line $\overline{u_r^2}$ and $\overline{u_\phi^2}$ are indistinguishable; we thus have $\overline{U_n^2} = \overline{u_r^2} + \overline{u_\phi^2} = 2\overline{u_r^2} = 2\overline{u_\phi^2}$, where r and ϕ are cylindrical co-ordinates appropriate to the jet.

Fluid-mechanical damping in the probe output pressure lines was controlled by the insertion of creeping-flow resistances, e.g. equal lengths of 0·2 mm inside diameter hypodermic tubing. Pressures were sensed with differential pressure transducers (first a Pace Engineering Co. Model P 90 D, and later a Datametrics Barocel Type 523). The time constant for 50 % response to a step change in pressure was adjusted to values between 15 s and 60 s. The electrical output was read with an integrating system, usually with an integration time of 100 s.

Table 3 gives the predicted relation between the normalized probe response $\Delta\bar{P}_s/(\bar{P}_{s1} - \bar{P}_b)$ and the turbulence level $v^2 \equiv \overline{U_n^2}/\bar{U}_x^2$. The hot-wire anemometer data of Wygnanski & Fiedler (1969) show that $\beta \simeq 1$, and we therefore adopt this value; the outcome, however, according to table 3, is about the same for any reasonable choice of β. The turbulence intensities so calculated from the differential Pitot measurements along the jet centre-line are shown in figure 15. The hot-wire data of Wygnanski & Fiedler, also shown, provide a comparison with the best results available by that technique. These authors measured $\overline{u_x^2}$, $\overline{u_r^2}$ and $\overline{u_\phi^2}$ in an air jet under operating conditions similar to ours, and their data appear to be of the highest quality that the current state of hot-wire anemometry allows. The good agreement between the results given by these totally different and independent techniques can be taken as strong evidence for the essentially validity and accuracy of both Any differences between the two sets of data are so nearly within the precision error of the measurements as to be of doubtful significance. It should be noted that the scatter in the present data, increasing in severity with downstream distance, simply reflects a precision error due to the limiting of the time averaging process, and could be reduced to any desired degree by increasing the effective averaging time. Wygnanski & Fiedler's difficulties in this regard were smaller because their nozzle was only one-third as large, but they also remarked on the long averaging times required to achieve high precision.

Another comparison with hot-wire measurements is afforded by the data of Curtet & Ricou (1964), who studied an axisymmetric ducted jet system at a Craya–Curtet number Ct of 4·5 (ratio of jet and duct diameters = 0·074; ratio

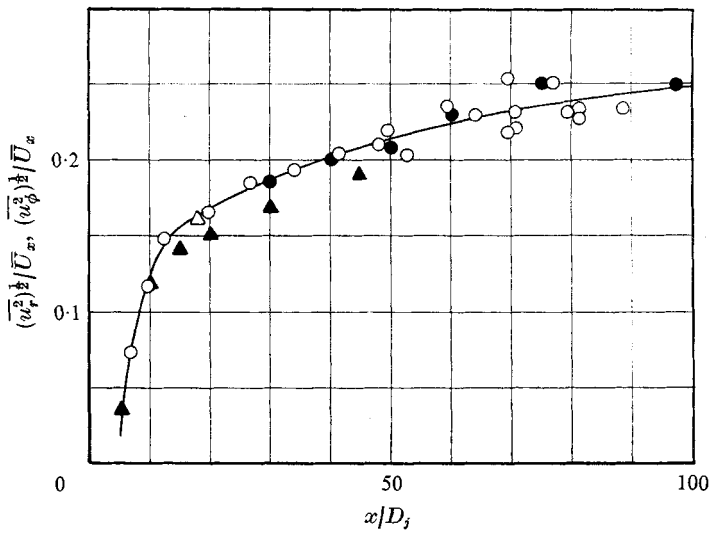

FIGURE 15. Turbulence characteristics on the centre-line of round jets. ○, free jet, from present measurements with differential Pitot probe; ●, free jet, hot-wire measurements of Wygnanski & Fielder (1969); △, confined jet with $Ct = 0{\cdot}345$, from present measurements with Pitot probes (data in figure 12); ▲, confined jet with $Ct = 4{\cdot}5$, hot-wire measurements of Curtet & Ricou (1964; in this case the ordinate is $(\overline{u_r^2})^{\frac{1}{2}}/(\overline{U}_x - U_f)$, where U_f is the free-stream velocity).

of nozzle and free-stream velocities in nozzle plane = 3·7). Their results indicate that $(\overline{u_x^2})^{\frac{1}{2}}/(\overline{U}_x - U_f)$, where $U_f(x)$ is the local free-stream velocity, is only weakly affected by Ct along the jet centre-line (until the jet reaches the duct wall), and the values obtained are very similar to those in a free jet. The same observation appears to apply to $(\overline{u_r^2})^{\frac{1}{2}}/(\overline{U}_x - U_f)$ (figure 15); Curtet & Ricou's hot-wire results lie quite near our differential Pitot data and Wygnanski & Fiedler's hot-wire data on free jets.

The centre-line value of the turbulence intensity given by the results in figure 12, measured with considerably smaller and different Pitot probes in a jet from a nozzle only $\frac{1}{12}$ as large, but with reasonably comparable boundary conditions and nozzle Reynolds number, agrees closely with the data on our large free jet (figure 15).

It may be concluded that the experimental evidence generally supports the present theory of Pitot response in turbulent streams. The greatest weight must be given to the good agreement with the hot-wire results of Wygnanski & Fiedler. To establish fully the validity of this critical comparison, we shall substantiate our earlier statement that Wygnanski & Fiedler's jet system was similar to ours, so similar, indeed, as to be virtually identical in behaviour over the critical region.

The throat diameter of Wygnanski & Fiedler's nozzle was 2·7 cm and the exit air velocity was about 68 m/s, compared with our values of 7·5 cm and 55 m/s. The exit Mach numbers were thus virtually equal, about $M = 0{\cdot}20$. The exit Reynolds numbers, $Re = 1{\cdot}0 \times 10^5$ and $2{\cdot}5 \times 10^5$, were large and similar in value. Both nozzles were designed to give a uniform exit velocity distribution

except in the wall boundary layer, which, at these Reynolds numbers, is of negligible thickness. The studies of Laurence (1956), Davies, Fisher & Barratt (1963), Kolpin (1964) and Becker & Massaro (1968) show that under these conditions any differences between the jets, attributable to the effects of exit velocity distribution, Mach number and Reynolds number, should be quite imperceptible.

Wygnanski & Fiedler's nozzle was set with its mouth in the plane of a 2 m square wall and ours was set in a 1 m square wall. The diameter of the bounding wall at $x = 0$ (the plane of the nozzle mouth) was in both cases over 10 times the nozzle diameter. The flow beyond the wall edge was therefore of very low velocity relative to fluid in the jet, and so the wall acted like an infinite plane at $x = 0$ (extending to $r \to \infty$ in the cylindrical co-ordinate system of the jet).

Conditions in the nozzle plane $x = 0$ in our work and Wygnanski & Fielder's were thus so similar that no significant difference between the jets can be expected from this source. Consider, finally, the boundary conditions at $x > 0$, and particularly at $x \gg D_j$. Far enough downstream, as velocities in a jet decay to levels approaching those of room draughts and as the confining effect of the room begins to be felt, departures from the desired boundary condition $U \to 0$ as $r \to \infty$ must exert a disturbing influence. Wygnanski & Fiedler took precautions so that disturbances were considered to be small as far downstream as $x = 100D_j$. Our measurements were done in a very large room under highly uniform temperature conditions and with the ventilation system turned off. The first significant downstream disturbance arose from the fact that the nozzle was aimed horizontally about 1·3 m above the laboratory floor. The free jet thus approached the floor around $x = 80D_j$ and then began undergoing transition into a wall jet. It may be concluded that the far-downstream boundary conditions in both our jet and Wygnanski & Fiedler's closely approximated ideality, with respect to any effect on centre-line turbulence properties, up to at least $x = 80D_j$.

If the boundary conditions remained ideal very far downstream, the properties of the turbulent field should closely approach a state of self-preservation. The centre-line value of $(\overline{u_r^2})^{\frac{1}{2}}/\overline{U}_x$ or $(\overline{u_\phi^2})^{\frac{1}{2}}/\overline{U}_x$ to which the free jet tends in self-preservation is not well defined in figure 15. A better basis for evaluating the trend is provided by figure 16. The same technique has previously been applied to data on concentration fluctuations (Becker *et al.* 1967, figure 7). The equation of the straight line which fits the data for $\overline{U}_x < 0{\cdot}25U_j$, or $x > 25D_j$, is

$$(\overline{u_r^2})^{\frac{1}{2}}/\overline{U}_x = (\overline{u_\phi^2})/\overline{U}_x = 0{\cdot}275(1 + 2{\cdot}3\overline{U}_x/U_j)^{-1}. \tag{39}$$

The hot-wire data of Wygnanski & Fiedler (1969) give, from figure 3 in their paper,

$$(\overline{u_x^2})^{\frac{1}{2}}/\overline{U}_x = 0{\cdot}287, \tag{40}$$

$x > 40D_j$. This indicates that, very nearly, $\overline{u_x^2} = \overline{u_r^2} = \overline{u_\phi^2} = 0{\cdot}28\overline{U}_x$ for $x \gg D_j$.

Characteristics of other differential probes

A more general impression of the turbulence detection characteristics of differential Pitot probes is conveyed by figure 17, which shows calculated values of $\Delta\overline{P}_s/\frac{1}{2}\rho\overline{U_n^2}$ as a function of $v^2 \equiv \overline{U_n^2}/\overline{U}_x^2$ for several probes. The probes considered

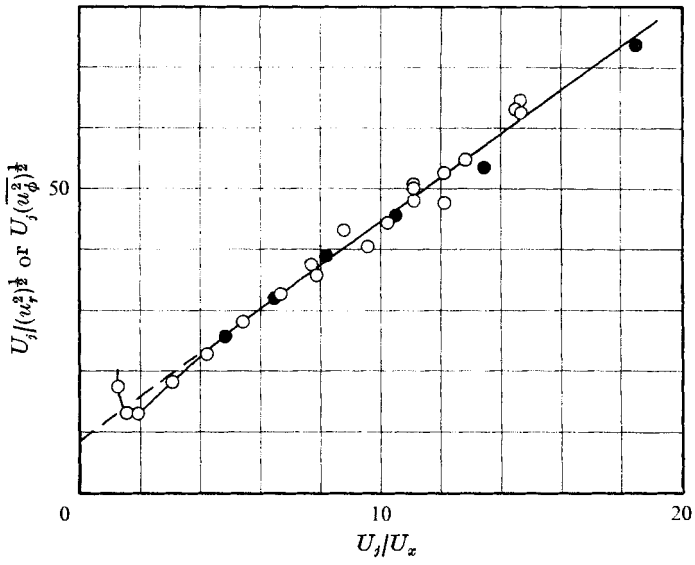

FIGURE 16. Trends in the intensity of the transverse components of velocity fluctuation on the centre-line of a free jet. ○, present data from measurements with differential Pitot probe; ●, hot-wire data of Wynganski & Fielder (1969).

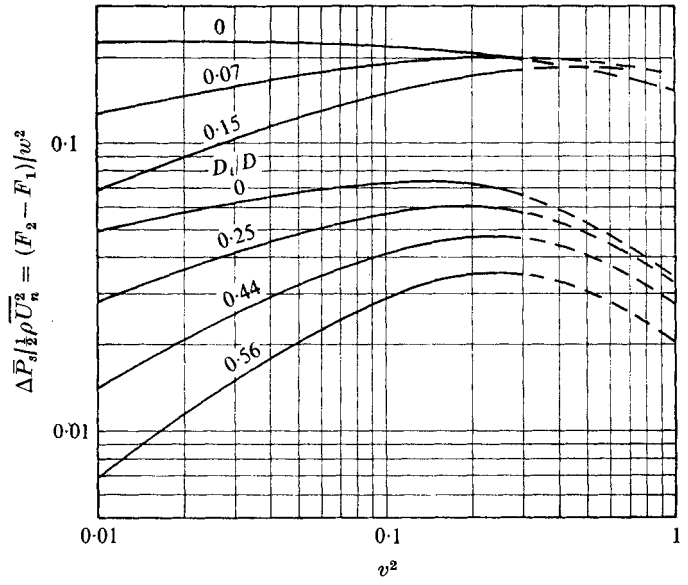

FIGURE 17. Response of differential Pitot probes having one component with $D_i/D = 1$. Top curves, other component is round-nosed; bottom curves, other component is square-nosed.

have the common feature that one component probe is a thin-walled tube, $1 - D_i/D \ll 1$. The other component is square-nosed or round-nosed. Sensitivity increases with decreasing values of D_i/D in the second component probe, and a round nose gives greater sensitivity than a square one.

7. Conclusion

The theory of Pitot probe response has so far been developed only for the following ideal operating conditions.

(i) Turbulence scale large, roughly $\Lambda > 5D$.

(ii) Probe Reynolds number large, roughly $Re > 1000$.

(iii) Mach number small, roughly $M < 0{\cdot}5$.

(iv) Negligible effect of mean velocity gradients.

Some of the effects of non-ideality will be considered in another paper. The complications are, however, not easily amenable to quantitative treatment. The best plan for the user of Pitot probes is therefore to select a probe such that ideal conditions will be approached as closely as possible.

The performance visualized in the theory will be attained only if surging flow in the probe, in response to the turbulent field outside, is made negligible. The fluid in the probe must be effectively brought to stagnation. For gases, this requires that the volume of fluid in the measurement system, in the pressure transmission lines and the pressure sensing device, be adequately small, and that changes in this volume be small. The desired effect may also be achieved by inserting a suitable flow resistance not too far from the probe mouth (but not too near, according to the criterion $L_i > 3D_i$ given in § 2).

The laminar-flow response equation (5) is fairly exact, for the probes here considered, at values of θ up to around 60°. The accuracy however diminishes rapidly at higher values of θ. It follows that if, in a turbulent flow, significant energy is found in values of U_n^2/U^2 above 0·75, the present theory will fail. In statistical terms, the point at which this happens should be above

$$w^2 \equiv \overline{U_n^2}/\overline{U^2} = 0{\cdot}2, \quad \text{or} \quad v^2 \equiv \overline{U_n^2}/\overline{U}_x^2 = 0{\cdot}3.$$

When probes are used for turbulence measurements, individual calibration of the directional sensitivity is desirable if very accurate results are sought. This is especially true for very small probes whose inside and outside diameters may not be known with sufficient accuracy to fix precisely the values of the response parameters m and K. Another source of error, the displacement effect in a velocity gradient (Hall 1956; Lighthill 1957), can be minimized by using square-nosed probes of equal outside diameter. The residual displacement effect on the differential response is then reduced to a relatively weak influence of the diameter ratio D_i/D.

The highest differential response is however attained by coupling a round-nosed or sphere-nosed probe of small D_i/D with a square-nosed one of high D_i/D. Design criteria for the relative sizes of the probes to minimize the displacement effect have not been adequately determined, but there are indications that the outside diameter of the round-nosed or sphere-nosed probe should be between 1·4 and 1·7 times that of the square-nosed probe. In any case, the displacement effect in most turbulent shear flows should be small if the turbulence scale is at least half an order of magnitude larger than the diameter of the largest probe, $\Lambda > 5D$.

We have shown that, using Pitot probes of nearly the minimum practical size

($D = 0{\cdot}5$ mm), apparently reliable velocity fluctuation intensity data are obtained on a jet at a section where the shear-layer thickness is of the order of 2 cm (velocity half-radius 1 cm). The evidence further indicates that good data would still be obtained if the shear-layer thickness were as small as 1 cm, at which point $\Lambda = 5D$. The turbulence scale in pipe flows is of the order of $\frac{1}{20}$ the pipe diameter. Thus the smallest pipe flow in which our theory should quantitatively apply has a diameter of the order of 5 cm. By comparison, hot-wire anemometry can be successfully applied to flows somewhat smaller than the limits in these examples, but not very greatly so.

Differential pressure transducers now available can detect signals as small as a 10^{-4} mm water column, which means that, in air at room temperature, values of $(\overline{U_n^2})^{\frac{1}{2}}$ of 0·5 cm/s are measurable. Such high resolution was not required in our work; an instrument with a water-column range of 2·5 cm and the capacity of detecting differential pressures as small as 0·01 mm was quite satisfactory. The work could also have been done with a good micromanometer.

The use of Pitot-static (combined Pitot and static pressure) probes should be avoided when possible, because of the unknown effect of turbulence on the static pressure reading. This limitation might be removed by an investigation of the effect of turbulence on the response of the common cylindrical, round-nosed static pressure probe. The theory of the response can be developed in an analogous manner to the present theory, but the basic equation for steady laminar flow will be different from (5).

The static pressure taps in such probes should be made small enough so that there is no significant surging through them, and of sufficiently large depth-to-diameter ratio so that the fluid comes to rest inside the pressure tap.

For turbulent shear flows that satisfy the boundary-layer assumptions, the reference pressure for impact pressure measurements should preferably be taken at the shear-layer edge. According to our theory, round-nosed probes with D_i/D about 0·45 and square-nosed probes with D_i/D about 0·15 will then detect $\frac{1}{2}\rho\overline{U}_x^2$ with good accuracy.

The general theory provides a basis for computing the effect of turbulence on the response of the five-hole Pitot probe. This device is capable of measuring the static pressure and the three velocity components in a laminar flow. It is, however, most commonly used in turbulent flows, often with very high levels of velocity fluctuation.

Another application of the theory is to the probe developed by Ebrahimi (1967), in which a condenser microphone is located inside the heads of the probe, facilitating detection of turbulent fluctuations in the signal pressure P_s. Equation (6) shows that the result will be simple only when $m \simeq 1$. The effect of the pressure transmission channel (the cavity between the probe mouth and the microphone or other pressure transducer) on the frequency response must also be considered; discussions may be found in a paper by Wad (1969) and in a manual published by Disa (*Transducer Manual*, 1969, Herlev, Denmark).

REFERENCES

ALEXANDER, L. G. T., BARON, T. & COMINGS, E. W. 1950 *University of Illinois Engng Exp. Station Tech. Rep.* no. 8.

BECKER, H. A. & BROWN, A. P. G. 1969 Velocity fluctuations in turbulent jets and flames. *12th Symp. (Int.) on Combustion*, p. 1059.

BECKER, H. A. & BROWN, A. P. G. 1972 Pitot response functions for turbulent flows. *Thermal & Fluid Sci. Group, Dept. Chem. Engng, Queen's University, Kingston, Ontario, Rep.* no. 2–72.

BECKER, H. A., HOTTEL, H. C. & WILLIAMS, G. C. 1963 *9th Symp. (Int.) on Combustion*, p. 842.

BECKER, H. A., HOTTEL, H. C. & WILLIAMS, G. C. 1967 *J. Fluid Mech.* **30**, 285.

BECKER, H. A. & MASSARO, T. A. 1968 *J. Fluid Mech.* **31**, 435.

BROWN, A. P. G. 1971 Structure of the round free turbulent propane–air diffusion flame. Ph.D. thesis, Queen's University, Kingston, Ontario.

CORRSIN, S. & UBEROI, M. S. 1950 *N.A.C.A. Rep.* no. 998.

CURTET, R. & RICOU, F. P. 1964 *Trans. A.S.M.E.* D**86**, 765.

DAVIES, P. O. A. L. 1957 *J. Fluid Mech.* **3**, 441.

DAVIES, P. O. A. L., FISHER, M. J. & BARRATT, M. J. 1963 *J. Fluid Mech.* **15**, 337.

EBRAHIMI, I. 1967 *Combustion & Flame*, **11**, 225.

EICKHOFF, H. 1969 *Chem. Ing. Tech.* **41**, 721.

GIBSON, M. M. 1963 *J. Fluid Mech.* **15**, 161.

GOLDSTEIN, S. 1936 *Proc. Roy. Soc.* A **155**, 570.

GRACEY, W., LETKO, W. & RUSSELL, W. B. 1951 *N.A.C.A. Tech. Note*, no. 2331.

HACKESCHMIDT, M. 1968 *Maschinenbautech.* **17**, H 4.

HALL, I. M. 1956 *J. Fluid Mech.* **1**, 141.

HINZE, J. O. 1959 *Turbulence*. McGraw-Hill.

HINZE, J. O. & VAN DER HEGGE ZIJNEN, B. G. 1949 *Appl. Sci. Res.* A **1**, 435.

KIEL, G. 1935 Total head meter with small sensitivity to yaw. *N.A.C.A. Tech. Mem.* no. 775. (Trans. from *Luftfahrt*, p. 75, 1935.)

KOPLIN, M. A. 1964 *J. Fluid Mech.* **18**, 529.

LAURENCE, J. C. 1956 *N.A.C.A. Rep.* no. 1292.

LIGHTHILL, M. J. 1957 *J. Fluid Mech.* **2**, 493.

MERRIAM, K. G. & SPAULDING, E. R. 1931 *N.A.C.A. Tech. Note*, no. 546.

MYADZU, A. 1936 *Ingen. Arch.* **7**, 35.

OWER, E. & JOHANSEN, F. C. 1926 *Aero. Res. Counc. R. & M.* no. 981.

PANKHURST, R. C. & HOLDER, D. W. 1952 *Wind-tunnel Technique*. London: Pitman.

RAY, A. K. 1956 *Ingen. Arch.* **24**, 171. (Trans. *Aero. Res. Counc. Rep.* no. 7, p. 498.)

WAD, G. 1969 *Disa Inf.* **7**, 25.

WYGNANSKI, I. & FIEDLER, H. 1969 *J. Fluid Mech.* **38**, 577.